Scientific Research Publishing

Atmospheric and Climate Sciences, 2026, 16(2), 358-376
https://www.scirp.org/journal/acs
ISSN Online: 2160-0422
ISSN Print: 2160-0414

Spatial-Temporal Variability of Frost Occurrence in Ethiopia during the ONDJ Season: Roles of ENSO and AO

Kedir Ali Hussen[1,2], Xin Geng[1*], Mulualem Abera Waza[1,3]

[1]Collaborative Key Laboratory of Meteorological Disaster, Ministry of Education (KLME), Joint International Research Laboratory of Climate and Environmental of Meteorological Disasters (CIC-FEMD), University of Information Science and Technology, Nanjing, China
[2]Amhara Regional State (ARS), Bahir Dar, Ethiopia
[3]Ethiopia Meteorology Institute (EMI), Addis Ababa, Ethiopia
Email: *gengxin@nuist.edu.cn

How to cite this paper: Hussen, K.A., Geng, X. and Waza, M.A. (2026) Spatial-Temporal Variability of Frost Occurrence in Ethiopia during the ONDJ Season: Roles of ENSO and AO. *Atmospheric and Climate Sciences*, **16**, 358-376.
https://doi.org/10.4236/acs.2026.162019

Received: February 16, 2026
Accepted: March 21, 2026
Published: March 24, 2026

Abstract

Frost events pose a critical climatic risk to agriculture and ecosystems in the Ethiopian Highlands. Yet, a quantitative understanding of the spatiotemporal variability and underlying climatic drivers remains elusive. In Ethiopia, frost occurs most frequently during the October-January (ONDJ) season, particularly in the central, southern, and northeastern highlands, where it exhibits high variability. This study investigates the spatiotemporal characteristics and climatic drivers of ONDJ frost days in Ethiopia. Trend analysis suggests a statistically significant decline in frost-day frequency across much of the highlands, consistent with the observed rise in minimum temperatures. EOF analysis identifies two leading modes of variability: a dominant, spatially uniform mode (EOF1, 64.1% of variance) and a secondary northwest-southeast dipole mode (EOF2, 11.98% of variance). The corresponding principal component time series (PC1 and PC2) both exhibit prominent interannual to near-decadal (4 - 10 years) variability. Further analysis indicates that while the PC1 is significantly positively correlated with ENSO (R = 0.41), the PC2 is strongly related to the extratropical Arctic Oscillation (AO) with a significant positive correlation coefficient (R = 0.36). El Niño induces an anomalous anticyclone over East Africa subjecting the Ethiopian highlands to dry, subsident conditions. The associated reduction in total cloud cover (TCC) enhances nocturnal radiative cooling, thereby increasing frost occurrence. In contrast, a positive phase of AO is associated with an anomalous cyclone over the northeastern Africa and Arabian Peninsula. This circulation favors subsidence in the northwest and ascent in the southeast, modulating TCC in opposing directions and

giving rise to a dipole pattern in frost-day frequency. Therefore, effectively integrating ENSO and AO signals into early warning and seasonal forecasting systems is critical for developing proactive adaptation strategies and improving frost-risk management in Ethiopia.

Keywords

Ethiopian Highlands, Frost Days, ONDJ Season, Trend Analysis, ENSO, Arctic Oscillation

1. Introduction

Ethiopia's physical geography, is shaped by complex topography, atmospheric circulation patterns, and global climatic forcing, giving rise to highly variable spatiotemporal weather and climate patterns. This is particularly evident across the country's dramatic elevation gradient, which ranges from 116 meters below sea level in the Danakil Depression to over 4500 meters above sea level in the Simien Mountains. Such extreme altitudinal variation produces sharp microclimatic gradients that strongly influence seasonal temperature extremes [1] [2]. The country experiences three rainy seasons: the Belg (February-May, FMAM), the Kiremt (June-September, JJAS), and the Bega (October-January, ONDJ). During the Bega season, the southward migration of the Intertropical Convergence Zone (ITCZ) brings higher rainfall to southern and southeastern Ethiopia. Concurrently, the highlands are influenced by relatively cool, dry northerly winds associated with the intensification of the Siberian High during the Northern Hemisphere winter [1] [3]-[5].

High elevation regions are particularly vulnerable during the ONDJ season, when clear skies and intense nocturnal radiative cooling frequently drive nighttime temperatures below freezing. These frost events have devastating consequences for agriculture, especially for frost-sensitive staple crops, such as teff, barley, and wheat. However, the complex interplay between local microclimates and large-scale climatic teleconnections renders frost occurrence inherently difficult to predict, often resulting in sudden and severe crop losses for farmers [6].

Global climate modes, particularly the El Niño-Southern Oscillation (ENSO), exert a strong influence on Ethiopia's seasonal climate. The alternating warm (El Niño) and cold (La Niña) phases of ENSO perturb tropical temperature and rainfall patterns, with well-documented impacts on Kiremt rainfall [7]-[10]. Despite the significant effects of frost on ecosystems and agriculture, the role of ENSO and the Arctic Oscillation (AO) in modulating ONDJ frost variability remains poorly understood. This gap has constrained the development of reliable early warning systems and region-specific adaptation strategies for frost-prone farming areas in Ethiopia.

Observational evidence indicates a rise in warm nights (TN90p) and annual minimum temperatures (TNn), alongside a decline in cool nights (TN10p), sug-

gesting a reduction in the frequency of very cold nights [11]. Given the critical importance of frost-sensitive crops to Ethiopia's highland agriculture, a more nuanced understanding of frost patterns is essential for designing effective mitigation and adaptation measures. To address these gaps, this study investigates the spatiotemporal dynamics of ONDJ frost events from 1981 to 2022, with a focus on their teleconnections with ENSO and AO. By examining how large-scale climate variability manifests locally in Ethiopia's complex highland topography, the study aims to advance understanding of frost drivers and support the development of improved forecasting and risk management tools. The remainder of the paper is organized as follows: Section 2 describes the data and methodology, Section 3 presents the results and discussion, and Section 4 summarizes the main conclusions.

2. Data and Methods

2.1. Study Area

Ethiopia is a landlocked country situated in the Horn of Africa, between 3˚N-15˚N and 33˚E-48˚E. It borders Eritrea to the northeast, Djibouti and Somalia to the east, Sudan and South Sudan to the west, and Kenya to the south. With an area of approximately 1,104,300 km^2, it is the seventh-largest country in Africa [12]. Topography exerts a dominant control over Ethiopia's climatic and ecological diversity. Elevations range from 100 meters below sea level in the Afar Depression to 4620 meters above sea level at Ras Dashen, with nearly two-thirds of the country situated above 1500 meters (**Figure 1(a)**, and **Figure 1(b)**) [13]. This dramatic altitudinal gradient supports a mosaic of environments from the desert-like

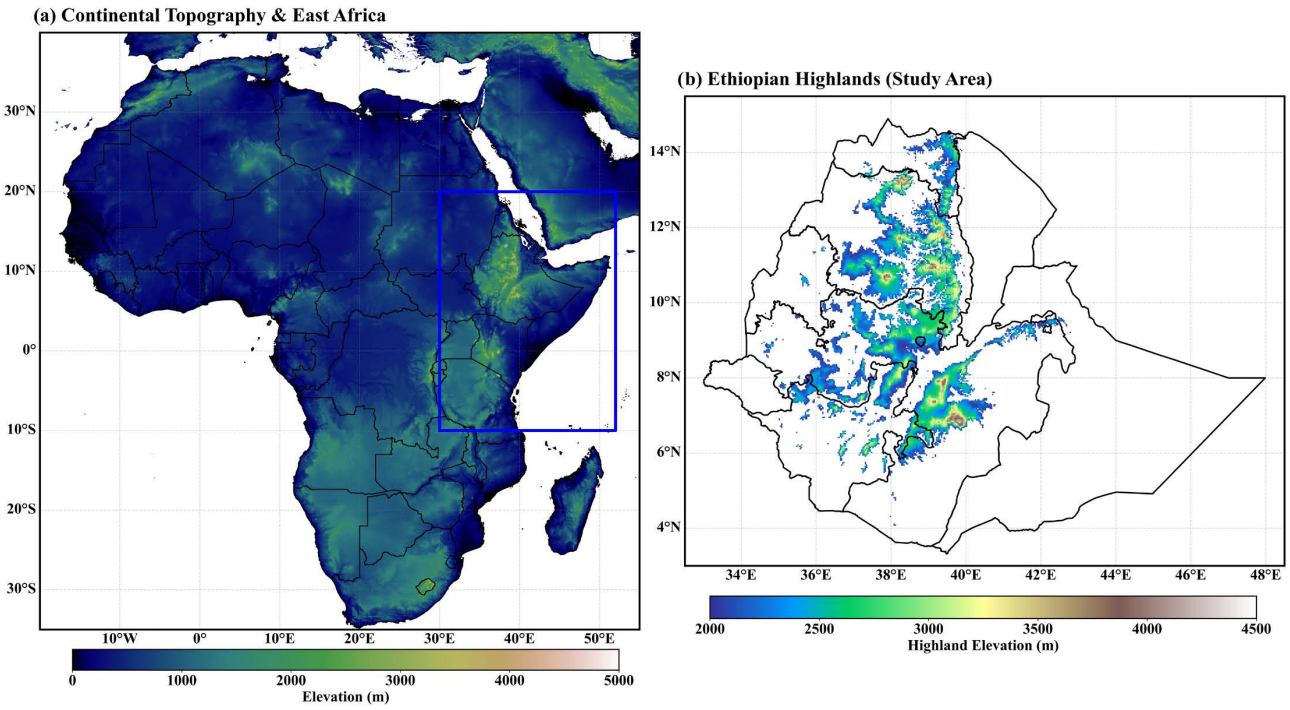

Figure 1. (a) Digital Elevation Model (DEM) geographical information for Africa, and (b) DEM for the Ethiopian Highlands (Units: meters).

lowlands of the northeast and southeast, through the temperate highlands of the central plateau, to the equatorial rainforests of the southwest. The Great Rift Valley further dissects the landscape, cutting diagonally across the country and creating a chain of escarpments and lakes.

Ethiopia's climate reflects this topographic complexity, shaped further by the seasonal migration of the Intertropical Convergence Zone (ITCZ). Traditional climate classification distinguishes three altitudinal belts: Dega (highlands), Woina-Dega (midlands), and Kolla (lowlands) [14]. Rainfall follows a pronounced spatial gradient, increasing steadily from the arid northeastern lowlands to the humid southwestern highlands.

2.2. Data and Methodology

Daily minimum temperature (Tmin) data for the period 1981-2022 were obtained from the Climate Prediction Center (CPC), providing gridded daily observations at 0.5˚ × 0.5˚ spatial resolution and widely used for analyses of temperature extremes [15] [16]. Sea surface temperature (SST) fields were derived from the Extended Reconstructed Sea Surface Temperature version 5 (ERSSTv5), available at 2˚ × 2˚ monthly resolution and commonly applied in studies of large-scale ocean-atmosphere variability [17]. Large-scale climate indices included the Niño-3.4 index, defined as area-averaged SST anomalies over 5˚S-5˚N and 120˚W-170˚W, the Arctic Oscillation (AO), and other relevant circulation indices obtained from NOAA sources. Atmospheric circulation variables, including Sea Level Pressure, horizontal and vertical winds, vertical velocity, were obtained from the NCEP/NCAR reanalysis dataset at 2.5˚ × 2.5˚ spatial resolution [18] [19]. We examined large-scale dynamical mechanisms related to ENSO and AO teleconnections using ERA5 reanalysis data from the European Center for Medium-Range Weather Forecasts (ECMWF). The variables examined included total cloud coverage (TCC) with a resolution of 0.25˚ × 0.25˚.

We define a frost day as a minimum temperature (Tmin) below 5˚C, consistent with agronomic studies showing that important Ethiopian highland crops, such as chickpea, wheat, and barley, experience growth inhibition and yield losses at minimum temperatures near or below this level, even without hard freezing [20]-[23]. Physiological phenology thresholds for these crops also suggest base temperatures near 5˚C, below which metabolic activity declines sharply. Using additional sensitivity thresholds of Tmin < 2˚C and Tmin < 0˚C confirms that the spatial trends and teleconnection patterns are robust to the specific frost definition, supporting the validity of the adopted threshold [24] [25]. ONDJ is defined as October-December of year Y and January of year Y + 1 (e.g., ONDJ 1981 = Oct-Dec 1981 and Jan 1982). All indices and atmospheric fields are averaged over the same ONDJ window. Temporal trends were evaluated using the non-parametric Mann-Kendall test, which is robust to non-normality and outliers, with trend significance assessed using the modified Mann-Kendall approach to account for serial correlation [26] [27]. Statistical significance of differences and regression patterns

was assessed using Student's t-test with effective degrees of freedom to correct for autocorrelation [28]. Teleconnection relationships between frost variability and large-scale climate indices were examined using Pearson correlation and linear regression, with significance adjusted for temporal dependence [29] [30]. Composite analysis was applied to contrast atmospheric and oceanic conditions during opposite ENSO and AO phases based on standardized index thresholds [31] [32]. We performed a multivariate regression of frost principal components (PCs) onto Niño3.4 and Arctic Oscillation (AO) indices simultaneously. An extended model also included the Indian Ocean Dipole (IOD) index. Each predictor's significance was assessed while controlling for the other(s) to evaluate independent contributions to frost variability. Wavelet power spectrum analysis was employed to identify dominant periodicities and their temporal evolution [33] [34]. Anomalies were computed relative to the 1981-2020 climatology, and linear trends were removed at each grid point. Data were weighted by the square root of cosine latitude to account for area differences. Only grid cells above 2005 m were included, and cells with >10% missing data were excluded; remaining gaps were interpolated. North's rule of thumb confirmed EOF1 and EOF2 are separable, justifying their interpretation as the dominant and secondary spatial patterns, respectively [35] [36].

3. Results and Discussions

3.1. Long-Term Climatology

Figure 2 illustrates the monthly evolution of mean frost days across the Ethiopian

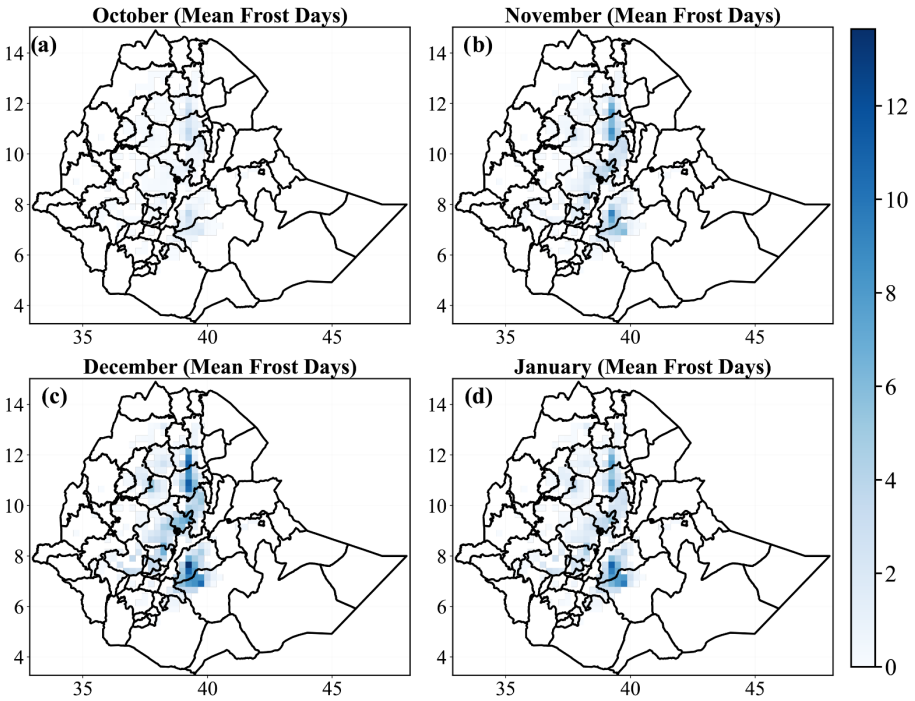

Figure 2. Spatial and seasonal progression of mean monthly frost days (days) over high-elevation regions of Ethiopia (>2005 m). (a) October, (b) November, (c) December, and (d) January. Shading indicates the average number of frost days per month.

Highlands (elevation > 2005 m) from October through January. The progression clearly demonstrates an intensification and expansion of frost coverage as the ONDJ season advances. In October (Figure 2(a)), frost is rare and spatially confined, marking the initial onset of cold conditions primarily at the highest elevations. By November (Figure 2(b)), the frequency of frost days increases, with a notable expansion across the central and northern highlands. Frost occurrence peaks in December (Figure 2(c)), during which widespread and frequent frost events affect most of the highland region. In January (Figure 2(d)), frost remains extensive but shows a slight reduction in intensity and a subtle spatial shift, signaling the gradual transition out of the peak frost season alongside increasing solar insolation. Collectively, the figure delineates a clear spatiotemporal progression of frost risk, with December representing the most critical period for frost exposure in the Ethiopian Highlands.

Figure 3(a), Figure 3(b) synthesize the spatial climatology and inter-annual variability of ONDJ frost days (defined as days with Tmin < 5˚C) for the Ethiopian

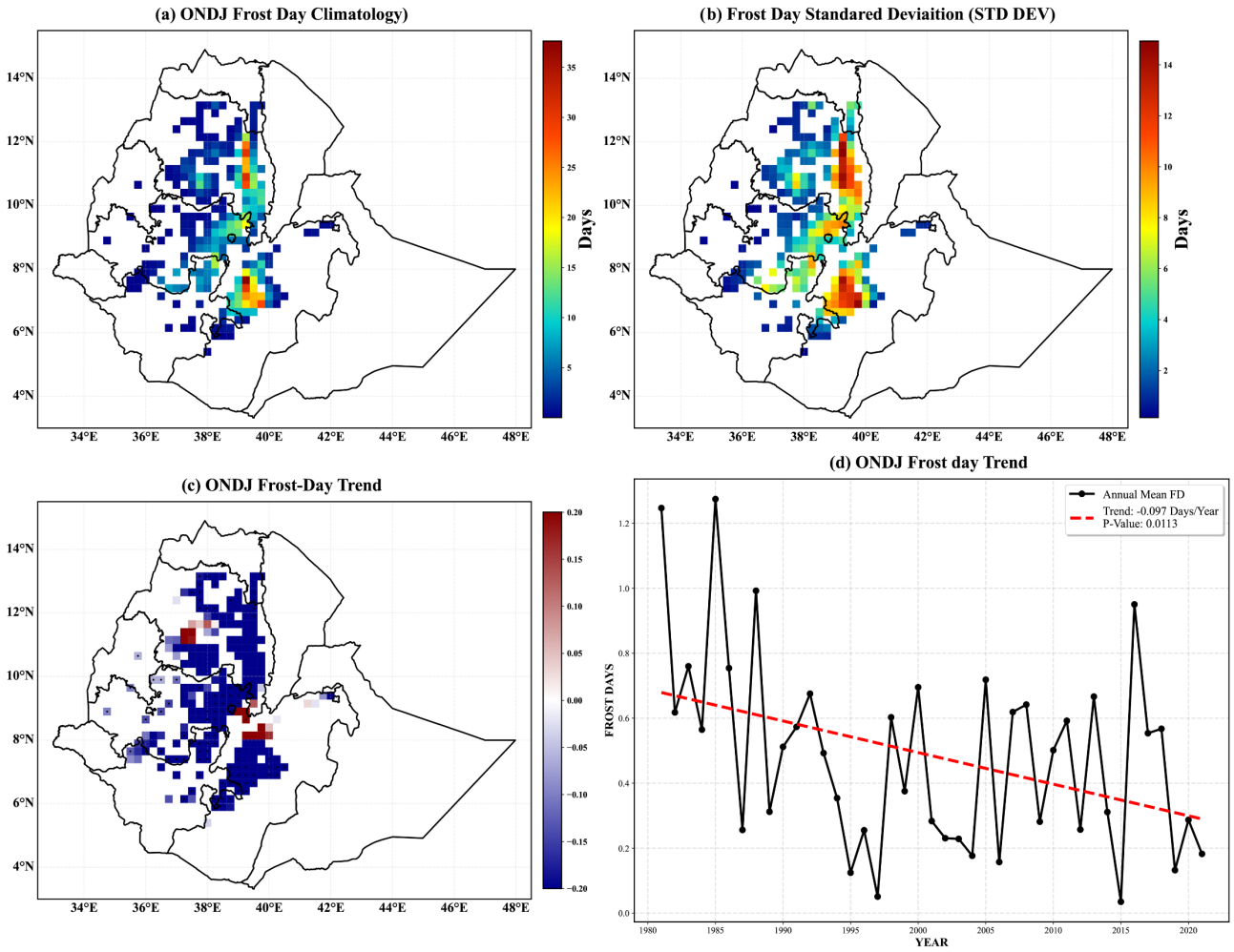

Figure 3. Characteristics of ONDJ frost days (defined as Tmin < 5˚C) over the Ethiopian Highlands (elevation > 2000 m): (a) mean climatology (days), (b) interannual variability (standard deviation, days), (c) spatial trends (days per year; stippling indicates significance at $p < 0.05$), and (d) regional mean time series with linear trend (days).

Highlands (>2005 m). The climatological mean pattern (Figure 3(a)) shows frost days concentrated in the central, southern, and northeastern highlands, with frequencies typically 25 - 40 days, while surrounding low-lying areas experience none. The pattern of standard deviation (Figure 3(b)), representing inter-annual variability reveals high variability (10 - 15 days) co-located with these same highland regions, indicating that the areas most prone to frost are also those where its year-to-year occurrence is most uncertain.

3.2. Trend Analysis

Figure 3(c) shows the spatial pattern of linear trends in frost days across the country during the 1981-2022 period. A dominance of negative trends is observed throughout the highlands. The most pronounced and spatially coherent declines occur in the Central, Southern, and Northeastern Highlands. In contrast, the decline is somewhat less evident in the Northwestern and Eastern Highlands. Localized pockets of weak positive trends are noted in areas such as Eastern Shewa, West Gojam, and South Gonder. The regional mean time series (Figure 3(d)) corroborates this spatial pattern, revealing a statistically significant ($p < 0.05$) long-term reduction in frost days. The time series shows peak frequencies in the early 1990s, followed by a general decline in recent decades. This trend is consistent with the observed rise in regional minimum temperatures under ongoing climatic warming. The documented weakening of frost occurrence carries significant implications for highland agriculture, ecosystem dynamics, and the design of climate adaptation strategies in frost-prone regions.

3.3. Dominant Mode of ONDJ Frost Days Variability

Figure 4 presents the two leading EOF modes of ONDJ frost days in the Ethiopian Highlands during 1981-2022. The first mode (EOF1), explaining 64.13% of the total variance, represents the dominant structured pattern of variability, characterized by spatially coherent anomalies of the same sign across the major highland regions. This pattern reflects a large-scale, uniform variation in frost days over the country. The associated principal component (PC1) captures the temporal evolution of this mode, displaying strong multi-scale periodicity with a pronounced interannual-to-near-decadal oscillation (Figure 5(c)). The second mode (EOF2), accounting for approximately 11.98% of the variance, exhibits a pronounced southeast-northwest dipole structure. This pattern is marked by opposing anomalies, with negative values over the northwestern highlands and positive values over the southeastern highlands, including parts of Eastern Shewa. The corresponding PC2 describes the temporal variability of this dipole pattern and is dominated by periodicities in the 4 - 10 years band, with an average dominant period of about 6 years (Figure 5(b)).

Collectively, the EOF analysis reveals that while frost-day variability in the Ethiopian Highlands is predominantly governed by a large-scale, uniform pattern (EOF1), a significant fraction of the variance is associated with regional-scale

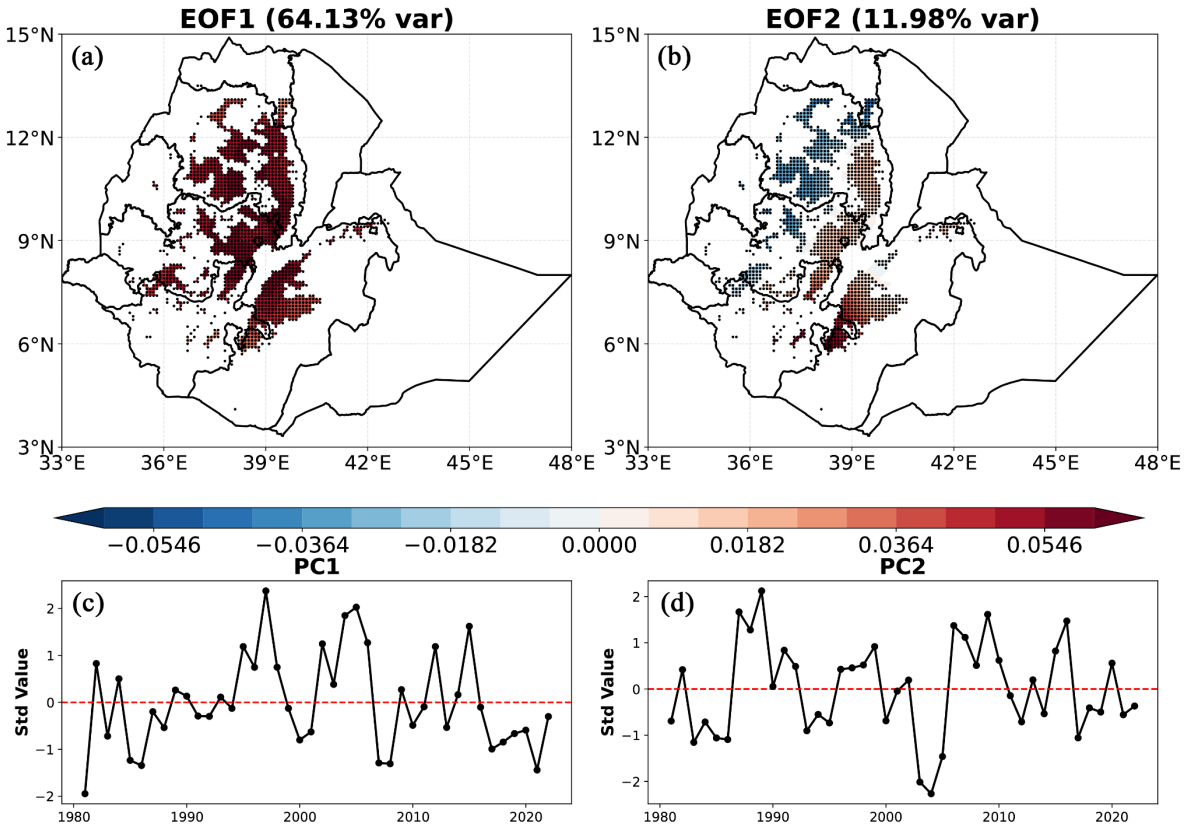

Figure 4. Leading EOF modes of ONDJ frost days over the Ethiopian Highlands (1981-2022): Spatial patterns of (a) EOF1 (64.13%) and (b) EOF2 (11.98%); significance ($p < 0.10$) is indicated by black dots. (c), (d) Corresponding standardized PC1 and PC2 time series.

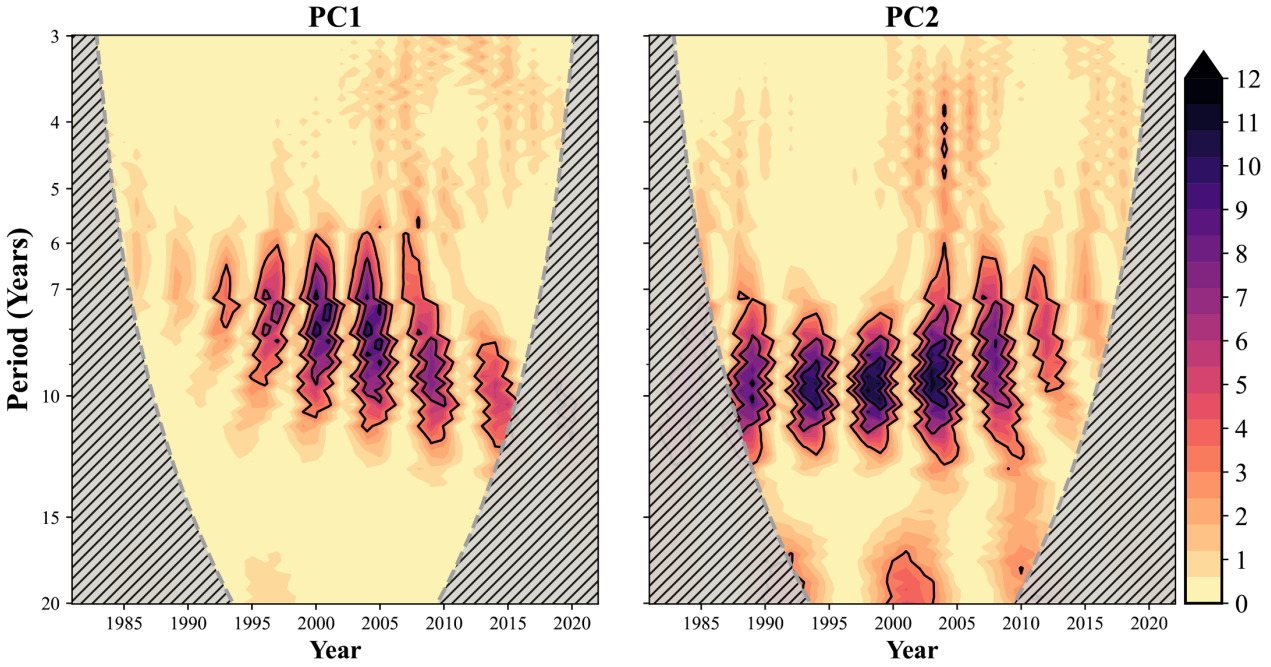

Figure 5. Continuous wavelet power spectra of (a) PC1 and (b) PC2 for ONDJ frost days over the Ethiopian Highlands (1981-2022). Black dashed contours indicate the ($p < 0.10$) confidence level against red noise; the shaded region denotes the cone of influence where edge effects may occur.

contrasts (EOF2), underscoring the importance of both coherent and opposing spatial modes in shaping the frost climate of the region.

3.4. Possible Mechanisms

Figure 6 elucidates the dynamical linkage between the dominant modes of ONDJ frost-day variability over the Ethiopian Highlands and large-scale ocean-atmosphere forcing. Regressions of global SST and sea level pressure (SLP) anomalies onto the leading principal components (PC1 and PC2) reveal coherent teleconnection patterns that drive regional frost dynamics.

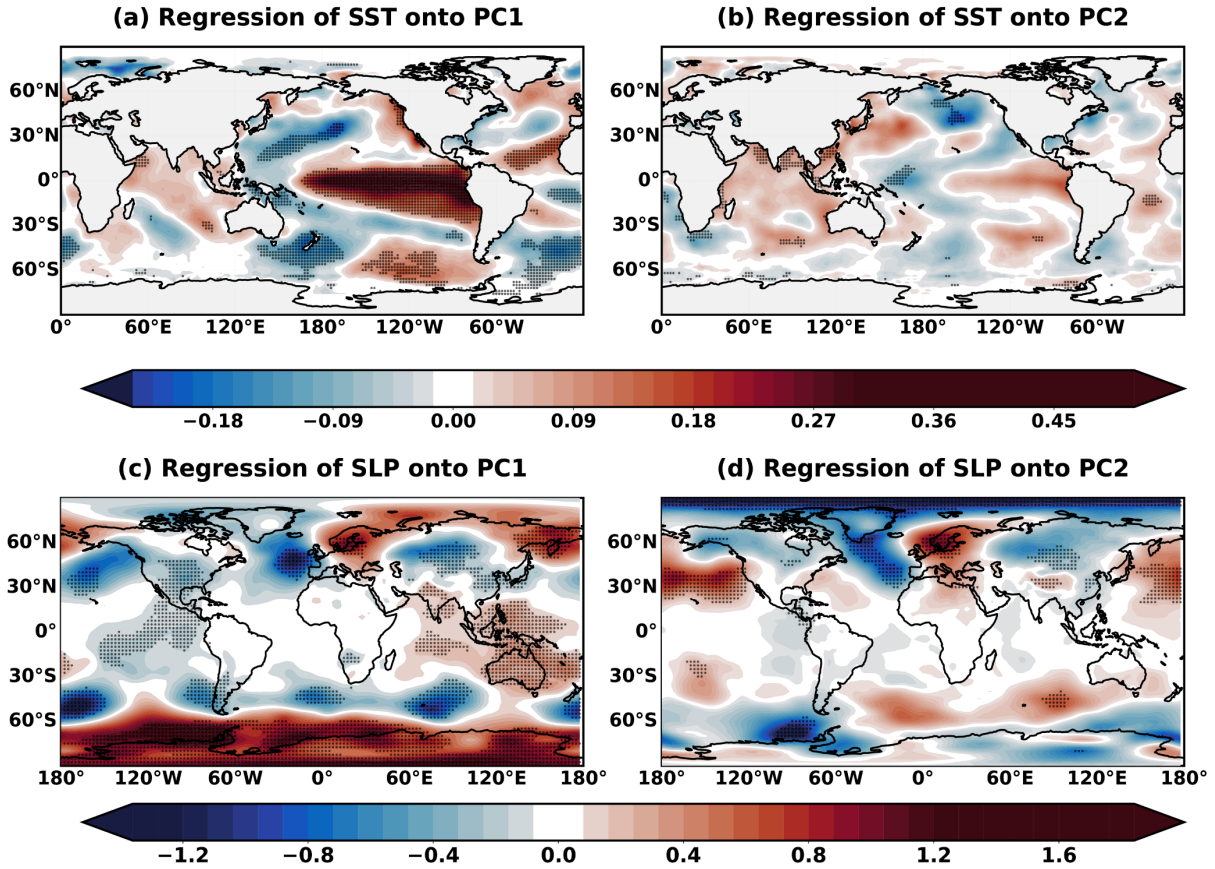

Figure 6. Regression of global SST (a), (b), units: ˚C and SLP (c), (d), units: hPa) anomalies onto the PC1 (a), (c) and PC2 (b), (d). Black dots denote the corresponding anomalies significant at the 95% confidence level ($p < 0.05$).

PC1, the dominant mode of coherent frost variability, exhibits a strong relationship with an El Nino-like SST pattern (Figure 6(a)), characterized by pronounced warming in the central-eastern equatorial Pacific (positive Niño 3.4 anomalies) and compensating cooling in the western Pacific and Southern Ocean. The corresponding SLP regression (Figure 6(c)) shows a weakened Walker circulation, marked by reduced pressure over the eastern Pacific and enhanced pressure over the Indo-western Pacific sector. This result suggests that when El Nino events occur, the frost occurrence tends to be enhanced across the whole Ethiopian Highlands.

PC2, which captures a spatial dipole frost pattern, is associated with inter-basin SST anomalies across the Indo-Pacific and Atlantic (Figure 6(b)). However, no statistically significant SST signal can be found. Its SLP signature (Figure 6(d)) reflects subpolar and mid-latitude pressure centers that modulate subtropical and mid-latitude circulation. This mode resembles the positive phase of the Arctic Oscillation (AO), suggesting that AO-related anomalies influence meridional cold-air advection into the region, thereby creating heterogeneous frost patterns across the highlands. These findings provide a crucial physical basis for improving seasonal frost forecasts, refining risk management, and supporting targeted agricultural adaptation in frost-vulnerable areas of Ethiopia.

Figure 7 summarizes the physical mechanisms through which ENSO affects ONDJ frost occurrence in the Ethiopian Highlands. The regression of 500-hPa

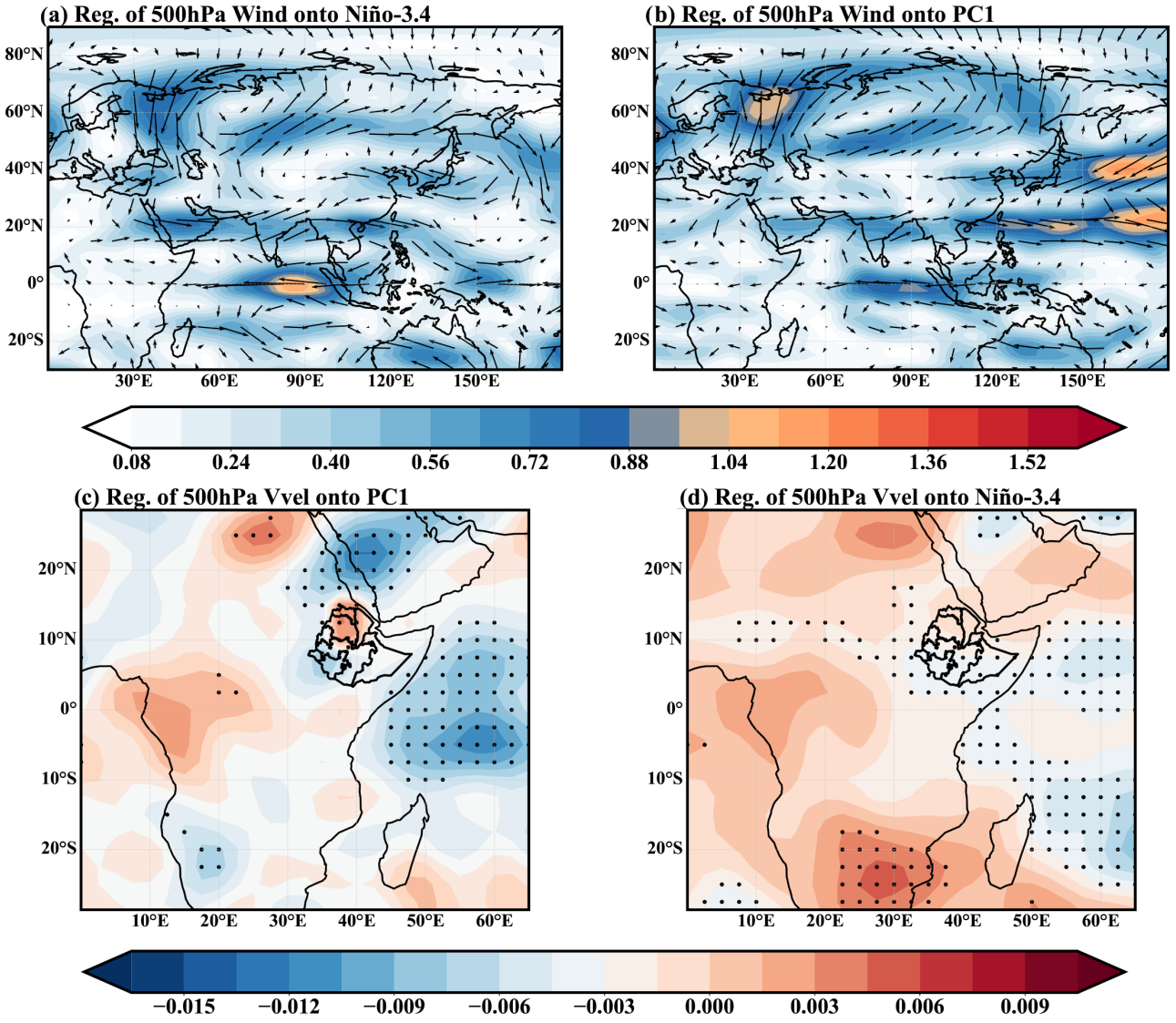

Figure 7. ENSO-related atmospheric circulation and vertical motion during ONDJ associated with frost variability over the Ethiopian Highlands. Regression of 500-hPa wind vectors onto (a) the Niño-3.4 index and (b) PC1. Regression of 500-hPa vertical velocity (Pa/s; negative/positive = ascent/descent) onto (c) PC1 and (d) Niño-3.4. Stippling (black dots) indicates significance at $p < 0.05$.

winds onto the Niño-3.4 index (Figure 7(a)) and PC1 (Figure 7(b)) reveals significant upper-level easterly anomalies over the eastern Indian Ocean during El Niño-like conditions. This indicates a weakened Walker circulation, which is characterized by suppressed convection, increased subsidence over the Indo-western Pacific, and a restructured equatorial pressure gradient. The anomalous easterly flow toward East Africa enhanced moisture inflow from tropical regions to southern and southeastern Ethiopia. Meanwhile, orographic blocking and westerly winds over northern Ethiopia and the Arabian Peninsula maintain dry, subsidence conditions in the central and northern highlands. The regression of 500-hPa vertical velocity on PC1 and Niño 3.4 (Figure 7) confirms that the strongest subsidence on PC1 (Figure 7(a)) favors clear skies, frost, and year-long cooling. In contrast, the Niño 3.4 regressions show more diffuse vertical velocity fields with divergent motion in the central and northern highlands (Figure 7(b)). This produces adiabatic airflow, which enhances nocturnal radiative cooling and increases frost frequency. Regressions of total cloud cover onto PC1 and Niño-3.4 (Figure 8(a) & Figure 8(b)) support this mechanism by showing reduced cloudiness over the central and northern highlands, which amplifies nighttime cooling. Meanwhile, cloud anomalies over southern and southeastern regions remain weak and spatially confined. The normalized time series (Figure 8(c)) confirms a statistically significant positive correlation between PC1 and Niño 3.4

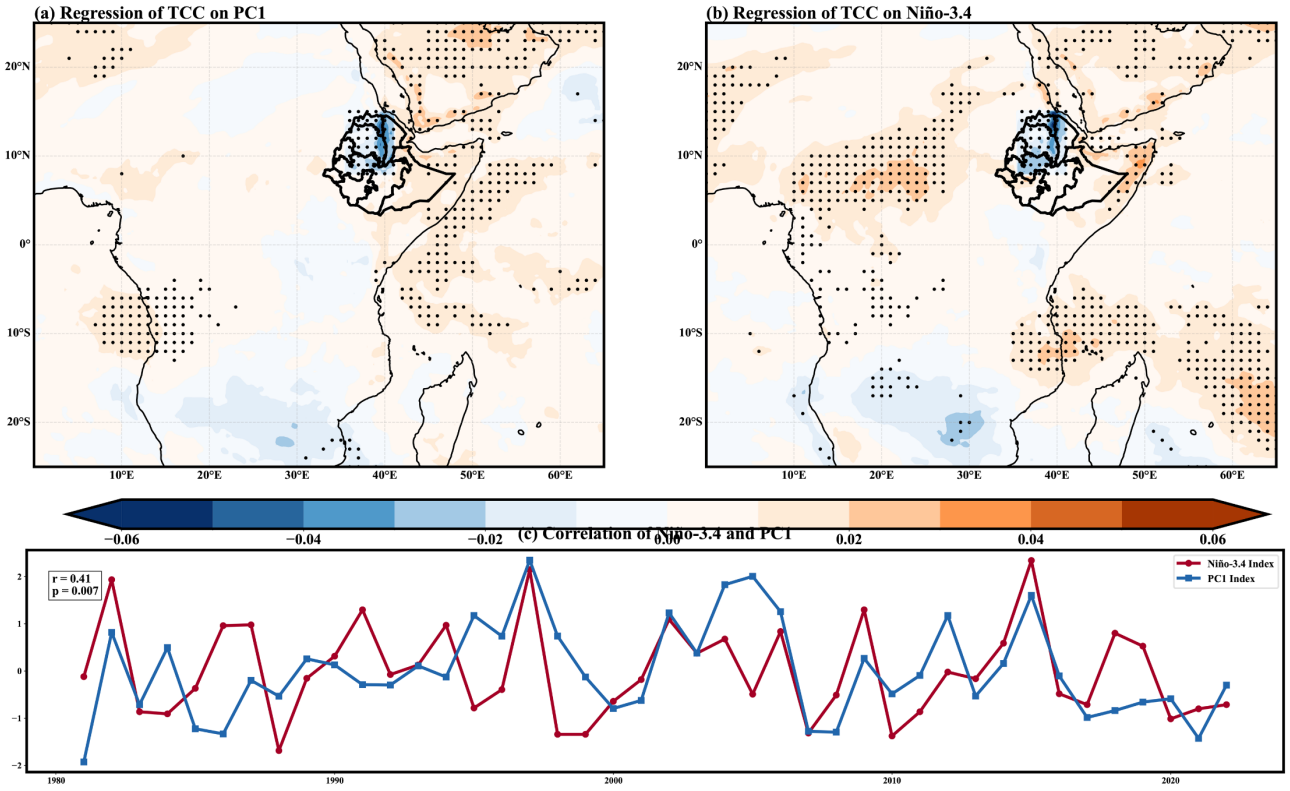

Figure 8. ONDJ total cloud cover (%) regressed onto (a) PC1 and (b) Niño-3.4 over the Ethiopian Highlands (1981-2022). Black dots denote significance at the 95% level. (c) Standardized time series of the Niño 3.4 index (red) and PC1 (blue), showing their relationship during 1981-2022.

(R = 0.41, $p = 0.007$). This supports the finding linking frost variability to ENSO forcing. The composite abnormal frost day time series also reflects the ENSO forcing relationships. El Niño years are characterized by statistically significant positive anomalies in most parts of the highland areas (Figure 9(a)), while La Niña years generally exhibit negative anomalies (Figure 9(b)). These anomalies align with high and low levels of moisture and cloud cover, modulating nocturnal cooling processes. Overall, the findings suggest that ENSO-associated circulation anomalies are reinforced by the effects of topography in the Ethiopian Highlands and cloud radiative effects, inducing more frequent frost events over the Ethiopian Highlands during ONDJ. Both Niño3.4 and AO remain significant, confirming independent contributions to frost variability; IOD inclusion does not alter these results.

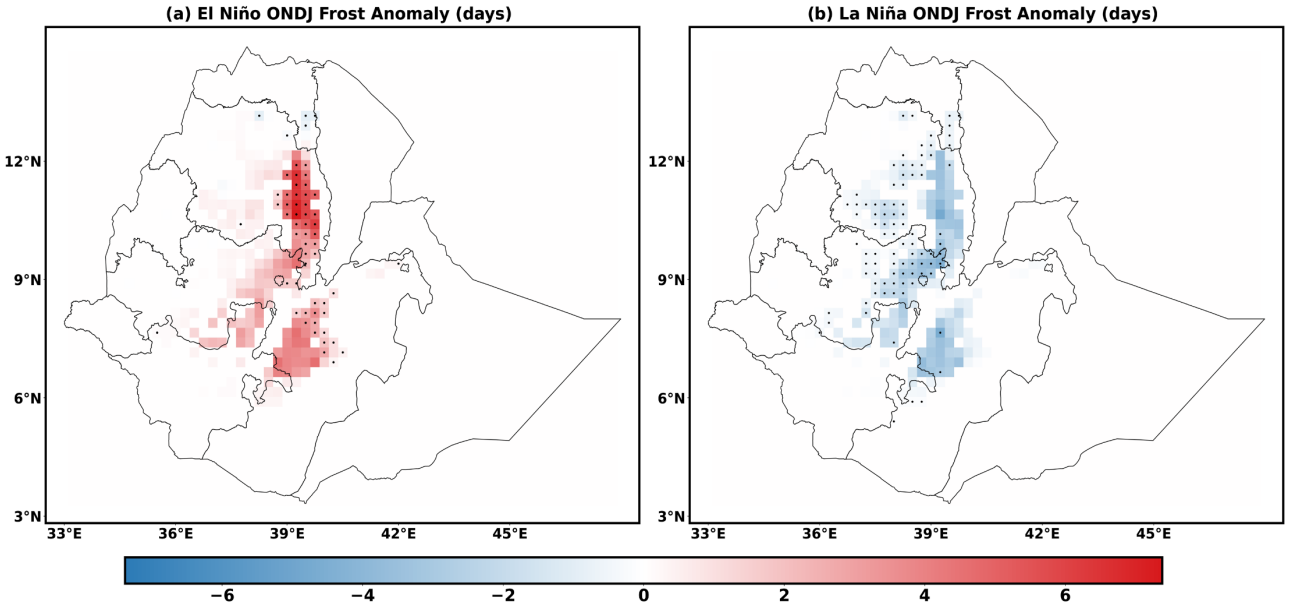

Figure 9. Composite anomalies of ONDJ frost days over the Ethiopian Highlands during (a) El Niño years and (b) La Niña years (1981-2022). Regions where the composite anomalies are statistically significant at the 95% confidence level are marked with black stippling.

Figure 10 elucidates the extratropical control of ONDJ frost variability over the Ethiopian Highlands via the Arctic Oscillation (AO). Regression of 500-hPa winds onto the AO index and PC2 (Figure 10(a) & Figure 10(b)) reveals a pronounced meridional dipole, with enhanced mid- to high-latitude westerlies over Eurasia and subtropical wind anomalies extending into the tropics, indicative of Rossby wave propagation and episodic southward incursions of cold, dry air into the Ethiopian Highlands. This dynamic control is reinforced in Figure 10(c) & Figure 10(d), showing the vertical velocity anomalies at 500 hPa associated with both PC2 and the AO, with strong upward motion dominant over the northern highlands, and weaker or subsidence motion over the central and southern regions. Corresponding regressions of total cloud cover onto PC2 and the AO index (Figure 11(a) & Figure 11(b)) show reduced cloudiness over the central and southern

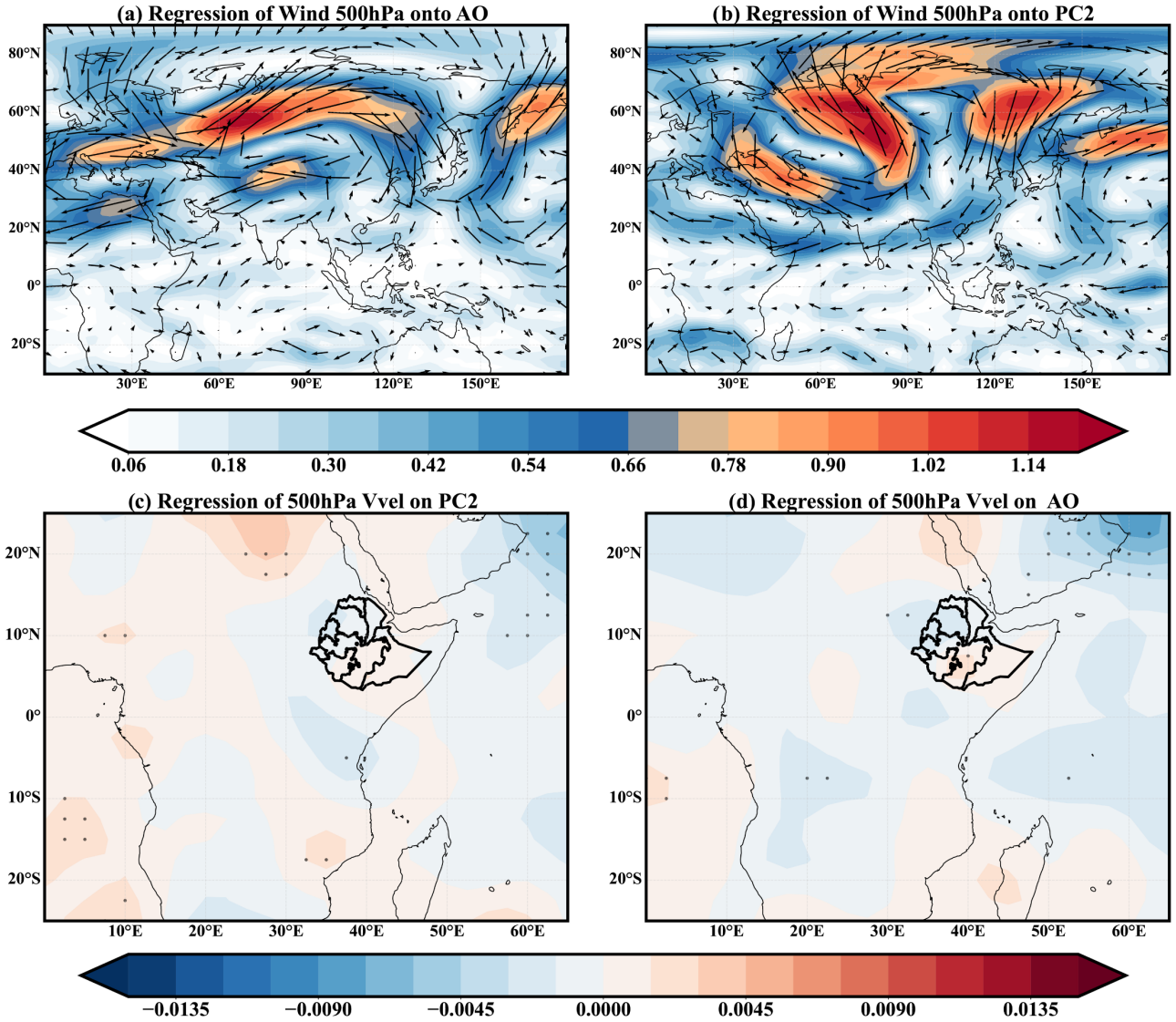

Figure 10. Arctic Oscillation-related ONDJ circulation associated with frost variability over the Ethiopian Highlands: 500-hPa wind regressions (m/s) onto (a) AO and (b) PC2; 500-hPa vertical velocity (Pa/s; negative/positive = ascent/descent) regressions onto (c) PC2 and (d) AO. Black dots denote significance at the 95% confidence level.

highlands and contrasting anomalies in the north, promoting dry adiabatic subsidence and amplified nocturnal radiative cooling. The standardized time series (Figure 11(c)) also show a statistically significant correlation between PC2 and AO index (r = 0.36, p = 0.018), indicating that the second mode of variability of frost is dynamically connected to AO forcing. Extending this dynamical view, Figure 12 illustrates the AO modulation of ONDJ frost day anomalies. During positive AO phases (Figure 12(a)), statistically significant positive frost day anomalies occur across the central, southern, and northeastern highlands, particularly along elevated escarpments. This pattern corresponds to strengthened northeasterly low-level flow, reduced moisture transport, clear skies, and strong radiative cooling conditions that favor frost formation. Conversely, during negative AO phases (Figure 12(b)), significant negative frost anomalies prevail over

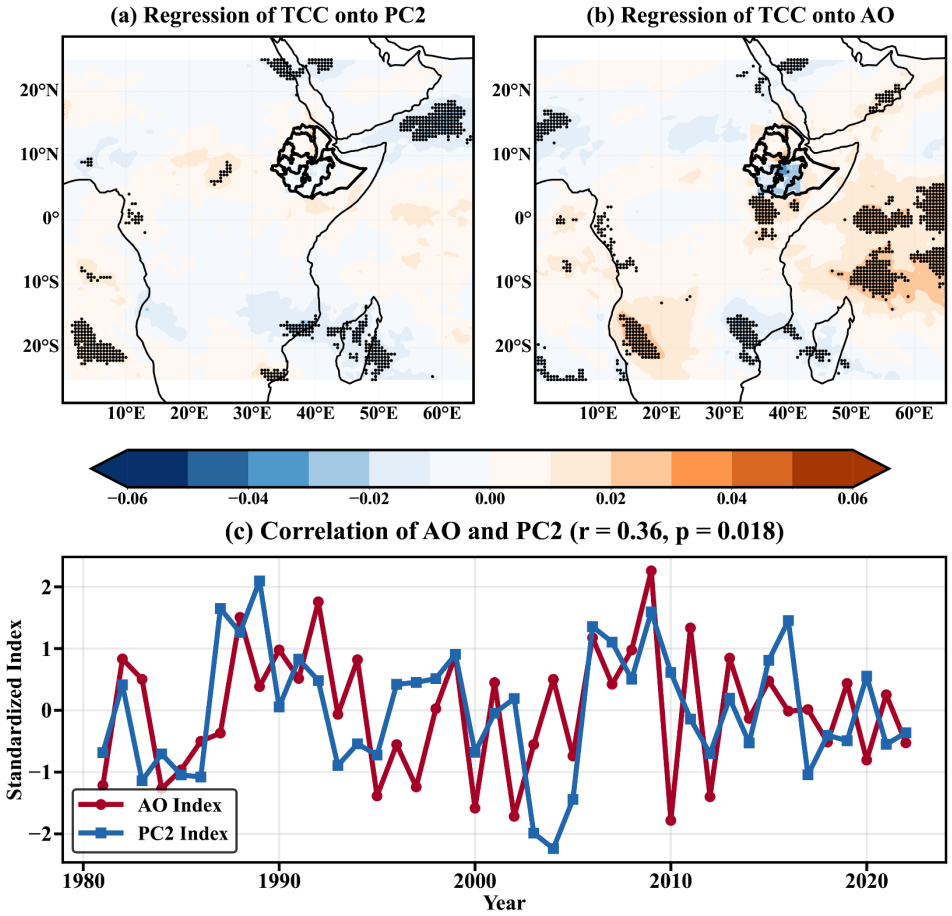

Figure 11. ONDJ total cloud cover (%) regressed onto (a) PC2 and (b) the Arctic Oscillation (AO) index over the Ethiopian Highlands. Black dots indicate statistical significance at the 95% confidence level. (c) Standardized time series of the AO index (red) and PC2 (blue) showing their relationship during 1981-2022.

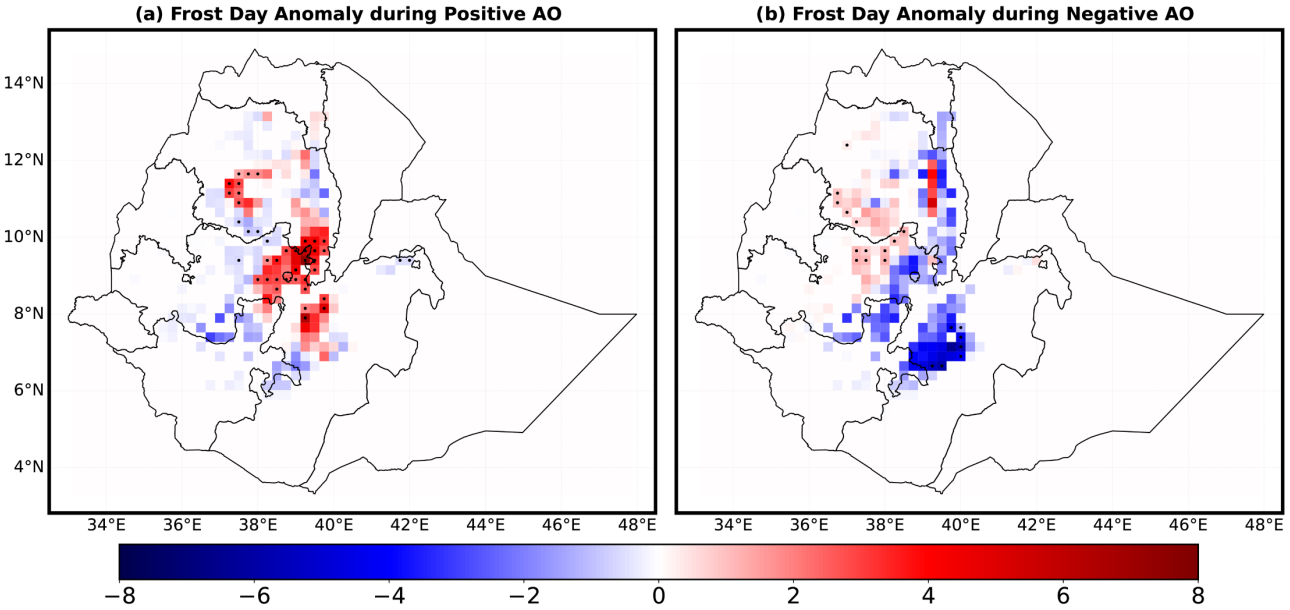

Figure 12. Composite maps of ONDJ frost days over the Ethiopian Highlands during (a) positive AO and (b) negative AO phases. Black stippling indicates areas that are statistically significant at the 95% confidence level.

the same regions, indicating reduced frost occurrence. These conditions are characterized by weakened north easterlies, increased moisture advection, and greater cloud cover, which collectively suppress nocturnal cooling and raise minimum temperatures. Overall, the analyses confirm that the circulation dipole associated with the AO primarily controls low-level winds, cloud cover, radiative cooling, and vertical motion, and secondarily controls ONDJ frost occurrence in the Ethiopian Highlands. Positive AO phases establish a dry, subsidence regime that increases the risk of frost, while negative AO phases create a thermodynamically buffered environment that inhibits frost development. The regression shows that Niño3.4 and AO each remain statistically significant after accounting for the other, confirming their independent influences on frost variability. Including IOD did not change the significance of ENSO and AO.

4. Summary and Conclusion

This study provides a comprehensive analysis of frost-day variability (T_{min} < 5˚C) during the ONDJ (October-January) period for the Ethiopian Highlands (>2005 meters) from 1981 to 2022. Climatologically, frost days occur most frequently in December, with 25 - 40 days at high elevations due to low moisture advection, low cloud cover, and high nocturnal radiative cooling. During the period 1981-2022, a significant reduction in frost day frequency is evident across most of the highlands ($p < 0.05$), particularly in the central and northeastern regions, consistent with the observed increase in minimum temperatures due to regional warming.

There exist two leading modes of the frost-day variability in Ethiopia. EOF1 shows a spatially uniform pattern and explains 64.1% of the total variance. EOF2 is a secondary northwest-southeast dipole mode and explains 11.98% of the total variance. They both exhibit prominent interannual to near-decadal variability. The ENSO signal is associated with EOF1 as indicated by the significant positive correlation with the Niño3.4 index (r = 0.41, $p = 0.007$). In contrast, EOF2 is associated with the extratropical forcing with a strong positive correlation with the Arctic Oscillation (r = 0.36, $p = 0.018$).

El Niño induces an anomalous anticyclone over East Africa, promoting dry, subsidence conditions and reduced cloud cover, which enhances nocturnal radiative cooling and increases frost occurrence. Conversely, a positive AO phase generates an anomalous cyclone over northeastern Africa and the Arabian Peninsula, producing opposing vertical motion anomalies, with subsidence in the northwest and ascent in the southeast that modulate cloud cover in opposing directions, giving rise to a dipole pattern in frost-day frequency.

Overall, ONDJ frost variability in the Ethiopian Highlands reflects the combined effects of long-term warming and episodic ENSO-AO-driven circulation anomalies. These results emphasize the importance of combining climate change trends and teleconnections in the development of early warning systems for frost events, agricultural risk management, and climate change adaptation plans in highland

regions that are susceptible to frost.

Acknowledgements

First and foremost, I would like to express my sincere gratitude to my supervisor, Prof. Xin Geng, for his insightful guidance, continuous support, and invaluable advice throughout the course of this research. His constructive feedback, helpful discussions, and patient supervision were essential to the successful completion of this study. His academic mentorship, encouragement, and careful monitoring greatly contributed to the quality and direction of this work. I extend my deepest gratitude to Mulualem Abera Waza for his extraordinary kindness, inspiration, and unwavering support throughout this study. I also gratefully acknowledge Nanjing University of Information Science and Technology (NUIST) for offering excellent research facilities and a supportive academic environment that were essential for the successful completion of this work. Finally, I would like to express my sincere gratitude to the Ministry of Commerce of the People's Republic of China (MOFCOM) for providing full scholarship support, which made this study possible.

Author Contributions

Prof. Xin Geng: Conceptualization, Project administration, Resources, Supervision, Methodology, Investigation, Formal analysis, Validation, Visualization, Writing—original draft, Writing—review & editing.

Kedir Ali Hussen: Conceptualization, Methodology, Software, Data curation, Investigation, Formal analysis, Validation, Visualization, Writing—original draft, Writing—review & editing.

Mulualem Abera Waza: Conceptualization, Methodology, Software, Formal analysis, Visualization, Writing—review & editing.

Funding Information

This research received no specific grant from any funding agency in the public, commercial, or not-for-profit sectors.

Data Availability

The study utilizes daily minimum temperature (Tmin) data from the Climate Prediction Center (CPC), covering the period from 1981 to 2022.
https://psl.noaa.gov/data/gridded/data.cpc.globaltemp.html

Monthly Extended Reconstructed SST Version 5.
https://iridl.ldeo.columbia.edu/SOURCES/.NOAA/.NCDC/.ERSST/.version5/.sst/

Niño-3.4 and Arctic Oscillation (AO) indices were obtained from the NOAA Physical Sciences Laboratory and NOAA Climate Prediction Center, respectively:
https://psl.noaa.gov/data/timeseries/month/Nino34_CPC/
https://www.cpc.ncep.noaa.gov/products/precip/CWlink/daily_ao_in-

dex/ao.shtml

Atmospheric circulation variables were obtained from ERA5.
https://cds.climate.copernicus.eu/datasets/reanalysis-era5-single-levels-monthly-means?tab=download

Conflicts of Interest

The authors declare no conflicts of interest regarding the publication of this paper.

References

[1] NMSA (National Meteorological Service Agency) (1996) Climatic and Agro-Climatic Resources of Ethiopia. NMSA Meteorological Research Report Series. V1, No. 1, Addis Ababa, 137 p.

[2] Gonfa, L. (1996) Climate classification of Ethiopia. Meteorological Research Report Series No. 3, National Meteorological Services Agency (NMSA), Addis Ababa, Ethiopia.
https://agris.fao.org/search/en/providers/122600/records/6472253177fd37171a72ad82

[3] Nicholson, S.E. (2017) Climate and Climatic Variability of Rainfall over Eastern Africa. *Reviews of Geophysics*, **55**, 590-635. https://doi.org/10.1002/2016rg000544

[4] Seleshi, Y. and Zanke, U. (2004) Recent Changes in Rainfall and Rainy Days in Ethiopia. *International Journal of Climatology*, **24**, 973-983.
https://doi.org/10.1002/joc.1052

[5] Korecha, D. and Barnston, A.G. (2007) Predictability of June-September Rainfall in Ethiopia. *Monthly Weather Review*, **135**, 628-650.
https://doi.org/10.1175/mwr3304.1

[6] Hurni, H. (1988) Degradation and Conservation of the Resources in the Ethiopian Highlands. *Mountain Research and Development*, **8**, 123-130.
https://doi.org/10.2307/3673438

[7] Camberlin, P., Moron, V., Okoola, R., Philippon, N. and Gitau, W. (2009) Components of Rainy Seasons' Variability in Equatorial East Africa: Onset, Cessation, Rainfall Frequency and Intensity. *Theoretical and Applied Climatology*, **98**, 237-249.
https://doi.org/10.1007/s00704-009-0113-1

[8] Nicholson, S.E. (2014) A Detailed Look at the Recent Drought Situation in the Greater Horn of Africa. *Journal of Arid Environments*, **103**, 71-79.
https://doi.org/10.1016/j.jaridenv.2013.12.003

[9] Gleixner, S., Keenlyside, N., Viste, E. and Korecha, D. (2016) The El Niño Effect on Ethiopian Summer Rainfall. *Climate Dynamics*, **49**, 1865-1883.
https://doi.org/10.1007/s00382-016-3421-z

[10] Mulualem Abera, W. and Wen, W. (2021) Interannual Variability of Seasonal Rainfall and Associated Circulations over Gambella, Ethiopia. *International Journal of Environmental Monitoring and Analysis*, **9**, 67-95.
https://doi.org/10.11648/j.ijema.20210903.13

[11] Worku, T., Khare, D. and Tripathi, S.K. (2018) Spatiotemporal Trend Analysis of Rainfall and Temperature, and Its Implications for Crop Production. *Journal of Water and Climate Change*, **10**, 799-817. https://doi.org/10.2166/wcc.2018.064

[12] Central Intelligence Agency (CIA) (2023) Ethiopia. In: The World Factbook.
https://www.cia.gov/the-world-factbook/about/archives/2023/countries/ethio-

pia/summaries/

[13] Fazzini, M., Bisci, C. and Billi, P. (2015) The Climate of Ethiopia. In: Billi, P., Ed., *Landscapes and Landforms of Ethiopia*, Springer, 65-87. https://doi.org/10.1007/978-94-017-8026-1_3

[14] Ministry of Agriculture (MoA) (2022) Agroecology: An Extension Training Manual. Ministry of Agriculture, Addis Ababa, Ethiopia. https://www.moa.gov.et/wp-content/uploads/2025/01/20220325_Agroecology-Manual.pdf

[15] Li, D., Zhou, T., Zou, L., Zhang, W. and Zhang, L. (2018) Extreme High-Temperature Events over East Asia in 1.5˚C and 2˚C Warmer Futures: Analysis of NCAR CESM Low-Warming Experiments. *Geophysical Research Letters*, **45**, 1541-1550. https://doi.org/10.1002/2017gl076753

[16] Lu, X., Yuan, C., Luo, J. and Yamagata, T. (2023) Delayed Impacts of ENSO on the Frequency of Summer Extreme Hot Days in the Asian Monsoon Region. Part II: Implication for Seasonal Prediction. *Journal of Climate*, **36**, 3113-3127. https://doi.org/10.1175/jcli-d-21-0668.1

[17] Huang, B., Thorne, P.W., Banzon, V.F., Boyer, T., Chepurin, G., Lawrimore, J.H., *et al.* (2017) Extended Reconstructed Sea Surface Temperature, Version 5 (ERS-STv5): Upgrades, Validations, and Intercomparisons. *Journal of Climate*, **30**, 8179-8205. https://doi.org/10.1175/jcli-d-16-0836.1

[18] Kalnay, E., Kanamitsu, M., Kistler, R., Collins, W., Deaven, D., Gandin, L., *et al.* (1996) The NCEP/NCAR 40-Year Reanalysis Project. *Bulletin of the American Meteorological Society*, **77**, 437-471. https://doi.org/10.1175/1520-0477(1996)077<0437:tnyrp>2.0.co;2

[19] Kistler, R., Collins, W., Saha, S., White, G., Woollen, J., Kalnay, E., *et al.* (2001) The NCEP-NCAR 50-Year Reanalysis: Monthly Means CD-ROM and Documentation. *Bulletin of the American Meteorological Society*, **82**, 247-267. https://doi.org/10.1175/1520-0477(2001)082<0247:tnnyrm>2.3.co;2

[20] Takele, R. (2023) Frost Hazard Map of Ethiopia. Ultimate Solutions Consultancy PLC.

[21] Admas, S., Haileselassie, T., Tesfaye, K., Shiferaw, E. and Flynn, K.C. (2021) Evaluation of Ethiopian Chickpea (*Cicer arietinum* L.) Genotypes for Frost Tolerance. *Acta agriculturae Slovenica*, **117**, 1-14. https://doi.org/10.14720/aas.2021.117.2.2079

[22] Chang-Yang, C., Sun, I., Tsai, C., Lu, C. and Hsieh, C. (2015) ENSO and Frost Codetermine Decade-Long Temporal Variation in Flower and Seed Production in a Subtropical Rain Forest. *Journal of Ecology*, **104**, 44-54. https://doi.org/10.1111/1365-2745.12481

[23] Crimp, S.J., Gobbett, D., Kokic, P., Nidumolu, U., Howden, M. and Nicholls, N. (2016) Recent Seasonal and Long-Term Changes in Southern Australian Frost Occurrence. *Climatic Change*, **139**, 115-128. https://doi.org/10.1007/s10584-016-1763-5

[24] Menzel, A., Seifert, H. and Estrella, N. (2011) Effects of Recent Warm and Cold Spells on European Plant Phenology. *International Journal of Biometeorology*, **55**, 921-932. https://doi.org/10.1007/s00484-011-0466-x

[25] Zhang, X., Alexander, L., Hegerl, G.C., Jones, P., Tank, A.K., Peterson, T.C., *et al.* (2011) Indices for Monitoring Changes in Extremes Based on Daily Temperature and Precipitation Data. *WIREs Climate Change*, **2**, 851-870. https://doi.org/10.1002/wcc.147

[26] Kendall, K. (1975) Thin-Film Peeling—The Elastic Term. *Journal of Physics D*: *Applied Physics*, **8**, 1449-1452. https://doi.org/10.1088/0022-3727/8/13/005

[27] Mondal, A., Kundu, S. and Mukhopadhyay, A. (2012) Rainfall Trend Analysis by Mann-Kendall Test: A Case Study of North-Eastern Part of Cuttack District, Orissa. *International Journal of Geology*, *Earth and Environmental Sciences*, **2**, 70-78.

[28] Helsel, D.R. and Hirsch, R.M. (2002) Statistical Methods in Water Resources. U.S. Geological Survey, Techniques of Water-Resources Investigations, Book 4, Chapter A3. https://doi.org/10.3133/twri04A3

[29] Wilks, D.S. (2011) Statistical Methods in the Atmospheric Sciences, Vol. 100. Academic Press.

[30] Montgomery, K.L., Vaughn, M.G., Thompson, S.J. and Howard, M.O. (2012) Heterogeneity in Drug Abuse Among Juvenile Offenders. Is Mixture Regression More Informative than Standard Regression? *International Journal of Offender Therapy and Comparative Criminology*, **57**, 1326-1346. https://doi.org/10.1177/0306624x12459185

[31] Von Storch, H. and Zwiers, F.W. (2002) Statistical Analysis in Climate Research. Cambridge University Press.

[32] Trenberth, K.E. (2019) El Niño Southern Oscillation (ENSO). *Encyclopedia of Ocean Sciences*, **6**, 420-432. https://doi.org/10.1016/b978-0-12-409548-9.04082-3

[33] Torrence, C. and Compo, G.P. (1998) A Practical Guide to Wavelet Analysis. *Bulletin of the American Meteorological Society*, **79**, 61-78. https://doi.org/10.1175/1520-0477(1998)079<0061:apgtwa>2.0.co;2

[34] Grinsted, A., Moore, J.C. and Jevrejeva, S. (2004) Application of the Cross Wavelet Transform and Wavelet Coherence to Geo-Physical Time Series. *Nonlinear Processes in Geophysics*, **11**, 561-566.

[35] Hsu, C.J. and Zwiers, F. (2001) Climate Change in Recurrent Regimes and Modes of Northern Hemisphere Atmospheric Variability. *Journal of Geophysical Research*: *Atmospheres*, **106**, 20145-20159. https://doi.org/10.1029/2001jd900229

[36] Hannachi, A., Jolliffe, I.T. and Stephenson, D.B. (2007) Empirical Orthogonal Functions and Related Techniques in Atmospheric Science: A Review. *International Journal of Climatology*, **27**, 1119-1152. https://doi.org/10.1002/joc.1499